euronoise 2021
25th to 27th of October
Madeira, Portugal - online

Determining the influence of the junction length on the vibration transmission across junctions

Wannes Stalmans[1], Cédric Van hoorickx[2] and Edwin Reynders[3]
KU Leuven
Kasteelpark Arenberg 40, 3001 Leuven, Belgium

ABSTRACT

Predicting the sound insulation between two spaces is a complex problem since it depends on both direct sound transmission through the separating element and on flanking transmission paths. When conventionally analyzing flanking transmission, a diffuse field is assumed in the walls and floors, which are modeled as plates, while junctions connecting walls and floors are assumed to be of infinite extent. In the present work, a new approach based on diffuse field reciprocity is proposed to account for the finite length of the junctions in a rigorous way, while still assuming diffuse vibration fields. This approach relies on the computation of the direct field dynamic stiffness matrices of the structural elements, which can be analytically derived for thin, isotropic plates or numerically determined with finite elements and perfectly matched layers for thick plates or more complex walls or floors. Using the new approach, practical design regression curves are determined where the length of the junction is considered.

1. INTRODUCTION

Effective protection from noise disturbance can be achieved by ensuring sufficient sound insulation in buildings. Unfortunately, this is a complex technical problem, since design details and multiple transmission paths can strongly influence the sound insulation [1]. Both the direct transmission through the element as well as the flanking transmission can impact the overall sound insulation between two rooms.

When conventionally analyzing flanking transmission, a diffuse field is assumed in walls and floors, which are modelled as plates. Junctions connecting the walls and floors are assumed to be infinite and the transmission of vibration across the junction is calculated by integrating the plane-wave transmission over all possible angles of incidence. Examples of this approach for homogeneous plate systems can be found in [2–4]. Up to now, it has not been investigated how this conventional approach can be adapted to take the finite junction length into account.

To address these limitations, an approach based on diffuse field reciprocity is proposed here. The diffuse field reciprocity relationship relates the blocked reverberant forces in a a vibrating subsystem at the junction to the direct field dynamic stiffness [5], i.e., the dynamic stiffness of the equivalent unbounded subsystem as observed at the finite junction. The direct field dynamic stiffness matrices in the wavenumber domain can be analytically derived for thin, isotropic, semi-infinite plates, as described by Langley and Heron [4]. Since the assumption of thin plates is only valid at low frequencies, another method is proposed here to determine the direct field dynamic stiffness using a combination of finite elements and perfectly matched layers. With this method a combination of 2.5D finite elements and perfectly matched layers is used to model a semi-infinite plate. The 2.5D finite elements allow modelling the 3D plate with a 2D mesh, taking into account that the

[1]wannes.stalmans@kuleuven.be

[2]cedric.vanhoorickx@kuleuven.be

[3]edwin.reynders@kuleuven.be

semi-infinite plate is unbounded along the junction. This is combined with a perfectly matched layer which absorbs outgoing waves to model the semi-infinite plate in the direction perpendicular to the junction.

In the presented work, both methods are used to calculate the direct field dynamic stiffness along the finite junction in the spatial domain by introducing a correction for baffled boundary conditions. Due to the computational efficiency of the new approach, vibration transmission across a large set of junction can be calculated. From the data acquired from these simulations, practical design regression curves are determined where the influence of the length of the junction is considered.

2. METHODOLOGY

2.1. Determination of transmission coefficient

A finite junction is considered with a junction length L and N plates connected to the junction which runs along the x-axis, as shown in Figure 1. The problem addressed in this paper is to calculate the transmission coefficient, which is defined as the ratio of the power transmitted through the junction from plate j to plate l to the power that is incident on the junction [1].

$$\tau_{jl} = \frac{W_{jl}}{W_{\mathrm{inc},j}} \tag{1}$$

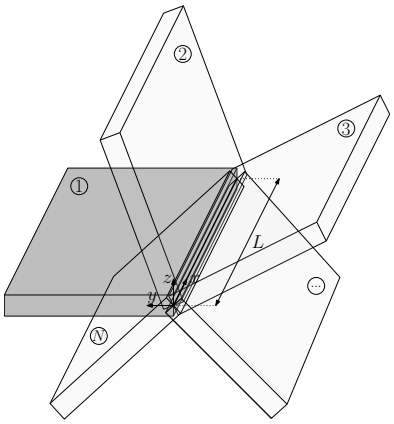

Figure 1: Number of plates connected to a finite junction with length L.

A new approach is presented here, in which the diffuse field transmission coefficient $\hat{\tau}_{jl}$ is calculated via the coupling loss factor $\hat{\eta}_{jl}$. The relation between these two is given by the following equation [6]

$$\hat{\tau}_{jl} = \frac{\omega\pi S_j}{c_{\mathrm{g},j} L}\hat{\eta}_{jl} \tag{2}$$

in which S_j is the surface area of plate j, $c_{\mathrm{g},j}$ is the group velocity of the considered wavetype in plate j and $\hat{\tau}_{jl}$ is the diffuse field transmission coefficient between the considered wave types of subsystems j and l.

The coupling loss factor can be determined with the following formula, which is derived using diffuse field reciprocity [5]

$$\hat{\eta}_{jl} = \frac{2\sum_{r,s} \mathrm{Im}\left(\mathbf{D}^{(l)}_{\mathrm{dir},rs}\right)\left(\mathbf{D}^{-1}_{\mathrm{tot}}\mathrm{Im}\left(\mathbf{D}^{(j)}_{\mathrm{dir}}\right)\mathbf{D}^{-\mathrm{H}}_{\mathrm{tot}}\right)_{rs}}{\omega\pi n_j} \tag{3}$$

in which $\mathbf{D}^{(j)}_{\mathrm{dir}}$ is the direct field dynamic stiffness matrix of subsystem j, $\mathbf{D}_{\mathrm{tot}} = \sum_{j=1}^{N_{\mathrm{s}}} \mathbf{D}^{(j)}_{\mathrm{dir}}$ where N_{s} is the total number of considered subsystems and n_j is the modal density of the considered subsystem of plate j:

$$n_j = \frac{S_j k_j}{2\pi c_{\mathrm{g},j}} \tag{4}$$

in which k_j is the wavenumber of the considered wavetype in plate j. Combining equations (2), (3) and (4), gives the expression below for calculating the diffuse field transmission coefficient,

$$\hat{\tau}_{jl} = \frac{4\pi}{Lk_j} \sum_{r,s} \mathrm{Im}\left(\mathbf{D}^{(l)}_{\mathrm{dir},rs}\right) \left(\mathbf{D}^{-1}_{\mathrm{tot}} \mathrm{Im}\left(\mathbf{D}^{(j)}_{\mathrm{dir}}\right) \mathbf{D}^{-\mathrm{H}}_{\mathrm{tot}}\right)_{rs} \tag{5}$$

Equation (5) shows that the diffuse field transmission coefficient for the transmission of bending waves depends on the junction length, the bending wavenumber of the excited plate and the direct field dynamic stiffness matrices of all plates that are connected to the junction. The direct field dynamic stiffness matrix is the dynamic stiffness of the equivalent unbounded subsystem as observed at the finite junction of a considered subsystem, and can be determined in multiple ways. Two possible methods will be discussed, where the first uses thin plate theory to analytically derive the direct field dynamic stiffness matrix of a thin, isotropic, semi-infinite plate in the wavenumber domain. A second method uses a combination of 2.5D finite elements and perfectly matched layers to determine the direct field dynamic stiffness matrix in the wavenumber domain. Both methods will be discussed next.

2.2. Derivation using thin plate theory

This section discusses the direct field dynamic stiffness matrix of a thin, isotropic, elastic semi-infinite plate in the wavenumber domain in the local coordinate system of the plate. The transformation from the wavenumber domain to the spatial domain will be discussed in section 2.4. Since the in-plane (IP) and out-of-plane (OOP) behavior of the plate are decoupled, the direct field dynamic stiffness matrix is a block diagonal matrix [4]

$$\mathbf{D}^{(j)'}_{\mathrm{dir}}(k_x) = \begin{bmatrix} \mathbf{D}^{(j)'}_{\mathrm{dir,IP}}(k_x) & \mathbf{0} \\ \mathbf{0} & \mathbf{D}^{(j)'}_{\mathrm{dir,OOP}}(k_x) \end{bmatrix} \tag{6}$$

$$\mathbf{D}^{(j)'}_{\mathrm{dir,IP}}(k_x) = \frac{E_j t_j}{k_x^2 - \mu_{\mathrm{S}}\mu_{\mathrm{L}}} \begin{bmatrix} -\frac{\left(\mu_{\mathrm{S}}^2 - k_x^2\right)\mu_{\mathrm{L}}}{2(1+\nu_j)} & \frac{-\mathrm{i}\left(\mu_{\mathrm{L}}^2 - \nu_j k_x^2\right)k_x}{1-\nu_j^2} + \frac{\mathrm{i}\mu_{\mathrm{S}}\mu_{\mathrm{L}}k_x}{1+\nu_j} \\ \frac{\mathrm{i}\left(\mu_{\mathrm{L}}^2 - \nu_j k_x^2\right)k_x}{1-\nu_j^2} - \frac{\mathrm{i}\mu_{\mathrm{S}}\mu_{\mathrm{L}}k_x}{1+\nu_j} & \frac{\left(\nu_j k_x^2 - \mu_{\mathrm{L}}^2\right)\mu_{\mathrm{s}}}{1-\nu_j^2} + \frac{k_x^2\mu_{\mathrm{S}}}{1+\nu_j} \end{bmatrix} \tag{7}$$

$$\mathbf{D}^{(j)'}_{\mathrm{dir,OOP}}(k_x) = E_j t_j \begin{bmatrix} \frac{\mu_{\mathrm{B1}}^3\mu_{\mathrm{B2}} - \mu_{\mathrm{B2}}^3\mu_{\mathrm{B1}}}{12\left(1-\nu_j^2\right)(\mu_{\mathrm{B1}} - \mu_{\mathrm{B2}})} & \frac{\mu_{\mathrm{B2}}^3 - \mu_{\mathrm{B1}}^3 + (1-\nu_j)(\mu_{\mathrm{B1}} - \mu_{\mathrm{B2}})k_x^2}{12\left(1-\nu_j^2\right)(\mu_{\mathrm{B1}} - \mu_{\mathrm{B2}})} \\ \frac{\mu_{\mathrm{B2}}^3 - \mu_{\mathrm{B1}}^3 + (1-\nu_j)(\mu_{\mathrm{B1}} - \mu_{\mathrm{B2}})k_x^2}{12\left(1-\nu_j^2\right)(\mu_{\mathrm{B1}} - \mu_{\mathrm{B2}})} & \frac{\mu_{\mathrm{B1}}^2 - \mu_{\mathrm{B2}}^2}{12\left(1-\nu_j^2\right)(\mu_{\mathrm{B1}} - \mu_{\mathrm{B2}})} \end{bmatrix} \tag{8}$$

where k_x is the wavenumber in the x-direction, E_j and ν_j are the Young's modulus and the Poisson's ratio of plate j, respectively, and

$$\mu_{\mathrm{L}} = -\sqrt{k_x^2 - k_{\mathrm{L}}^2} \qquad \mu_{\mathrm{S}} = -\sqrt{k_x^2 - k_{\mathrm{S}}^2} \tag{9}$$

$$\mu_{\mathrm{B1}} = -\sqrt{k_x^2 + k_{\mathrm{B}}^2} \qquad \mu_{\mathrm{B2}} = -\sqrt{k_x^2 - k_{\mathrm{B}}^2} \tag{10}$$

The longitudinal, transverse shear-wave, and bending wavenumbers can be calculated using respectively

$$k_{\mathrm{L}} = 2\pi f \sqrt{\frac{\rho_j\left(1-\nu_j^2\right)}{E_j}}, \tag{11}$$

$$k_{\mathrm{S}} = 2\pi f \sqrt{\frac{2\rho_j\left(1+\nu_j\right)}{E_1}}, \tag{12}$$

$$k_{\mathrm{B}} = \left(\frac{12\left(2\pi f\right)^2 \rho_j\left(1-\nu_j^2\right)}{E_j t_j^2}\right)^{\frac{1}{4}} \tag{13}$$

in which ρ_j and t_j are the density an thickness of plate j, respectively.

2.3. 2.5D finite elements with perfectly matched layers

The direct field dynamic stiffness of a plate can also be calculated using a combination of finite elements and perfectly matched layers, as shown in figure 2. Since the semi-infinite plate is infinite along the junction in the x-direction, a 2.5D approach can be applied to model the semi-infinite plate in the x-direction. The x-coordinate is transformed into the wavenumber k_x with a Fourier transform to allow representing the 3D response of the structure and the radiated wavefield on a two-dimensional mesh [7]. Since the semi-infinite plate extends to infinity in the positive y-direction, the 2.5D finite elements are combined with a perfectly matched layer. The perfectly matched layer surrounding the finite element model absorbs the wave propagating outwards from the bounded domain, thus simulating an unbounded subsystem [8]. A schematic representation of the model can be seen in figure 2. In the part of the plate where $0 \leq y \leq L_y$, quadratic 8-node elements are used which are coupled to the quadratic 8-node elements perfectly matched layer elements used in the part of the plate where $L_y \leq y \leq L_y + L_{\mathrm{PML}}$.

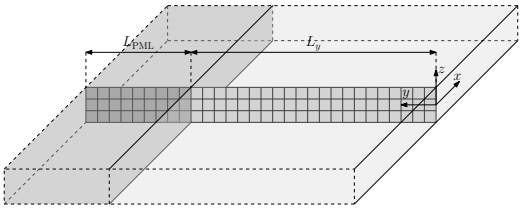

Figure 2: 2.5D model of a semi-infinite plate.

2.4. Transformation to the spatial domain of the direct field dynamic stiffness matrix

The finite length of the junction is taken into account in the transformation of the direct field dynamic stiffness matrices of the plates connected to the junction to the spatial domain. A method using a correction for baffled boundary conditions is introduced to calculate the direct field dynamic stiffness matrix of a semi-infinite plate in the spatial domain. The correction for baffled boundary conditions consists of first expressing the displacements of the junction as a linear combination of a set of shape functions

$$\mathbf{q} = \begin{bmatrix} u(x) \\ v(x) \\ w(x) \\ \theta(x) \end{bmatrix} = \sum_s q_s \boldsymbol{\phi}_s(x) \tag{14}$$

in which $\boldsymbol{\phi}_s$ is a vector with four components (translations in x-, y-, and z-direction and a rotation about the x-axis). The shape functions are constructed as follows

$$\begin{bmatrix} \boldsymbol{\varphi}_1 \\ \mathbf{0} \\ \mathbf{0} \\ \mathbf{0} \end{bmatrix}, \begin{bmatrix} \mathbf{0} \\ \boldsymbol{\varphi}_1 \\ \mathbf{0} \\ \mathbf{0} \end{bmatrix}, \begin{bmatrix} \mathbf{0} \\ \mathbf{0} \\ \boldsymbol{\varphi}_1 \\ \mathbf{0} \end{bmatrix}, \begin{bmatrix} \mathbf{0} \\ \mathbf{0} \\ \mathbf{0} \\ \boldsymbol{\varphi}_1 \end{bmatrix}, \begin{bmatrix} \boldsymbol{\varphi}_2 \\ \mathbf{0} \\ \mathbf{0} \\ \mathbf{0} \end{bmatrix}, \begin{bmatrix} \mathbf{0} \\ \boldsymbol{\varphi}_2 \\ \mathbf{0} \\ \mathbf{0} \end{bmatrix}, \ldots \tag{15}$$

in which φ_n is the nth sine function (sine functions are used since baffled boundary conditions are considered outside the junction):

$$\varphi_n(x) = \begin{cases} 0 & \text{if} \quad x < 0 \\ \sin\left(\frac{n\pi x}{L}\right) & \text{if} \quad 0 \leq x \leq L \\ 0 & \text{if} \quad x > L. \end{cases} \tag{16}$$

The shape functions φ_n are transformed from the spatial domain to the wavenumber domain. Due to the baffled boundary conditions the integration is limited from 0 to L.

$$\begin{aligned}\Phi_n\left(k_x\right) &= \int_0^L \varphi_n\left(x\right) \mathrm{e}^{-\mathrm{i}k_x x} \mathrm{d}x \\ &= \frac{\mathrm{e}^{\mathrm{i}\left(k_x - \frac{n\pi}{L}\right)L} - 1}{2\left(k_x - \frac{n\pi}{L}\right)} + \frac{1 - \mathrm{e}^{\mathrm{i}\left(k_x + \frac{n\pi}{L}\right)L}}{2\left(k_x + \frac{n\pi}{L}\right)}\end{aligned} \tag{17}$$

The corrected direct field dynamic stiffness matrix can now be calculated using [9]

$$\mathrm{D}_{\mathrm{dir},nm}^{(j)} = \frac{1}{2\pi} \int_{-\infty}^{\infty} \mathbf{\Phi}_n^{\mathrm{H}}\left(k_x\right) \mathbf{D}_{\mathrm{dir}}^{(j)}\left(k_x\right) \mathbf{\Phi}_m\left(k_x\right) \mathrm{d}k_x \tag{18}$$

in which $\mathbf{\Phi}_n$ is a vector with four component consisting of the shape functions in the wavenumber domain, $\mathbf{D}_{\mathrm{dir}}^{(j)}$ is defined in the global coordinate system and H is the Hermitian transpose. The direct field dynamic stiffness matrix $\mathbf{D}_{\mathrm{dir}}^{(j)'}$ is defined in the local coordinate system of plate j and has to be transformed to the global coordinate system [4]

$$\mathbf{D}_{\mathrm{dir}}^{(j)} = \mathbf{R}_j \mathbf{D}_{\mathrm{dir}}^{(j)'} \mathbf{R}_j^{\mathrm{T}} \tag{19}$$

where the transformation matrix $\mathbf{R}_j$ transforms the direct field dynamic stiffness matrix from the local coordinate system to the global coordinate system. Numerical integration is used for evaluating the integral in equation (18). The wavenumbers are sampled linearly; the number of samples and the upper limit wavenumber value are determined based on the convergence of the solution of the transmission coefficients.

3. RESULTS

The proposed approach will now be applied to an L-, T- and X-junction, as shown in figure 3. The materials used for the plates in the simulations can be found in table 1. The junction length is varied from 2 m to 8 m in steps of 1 m.

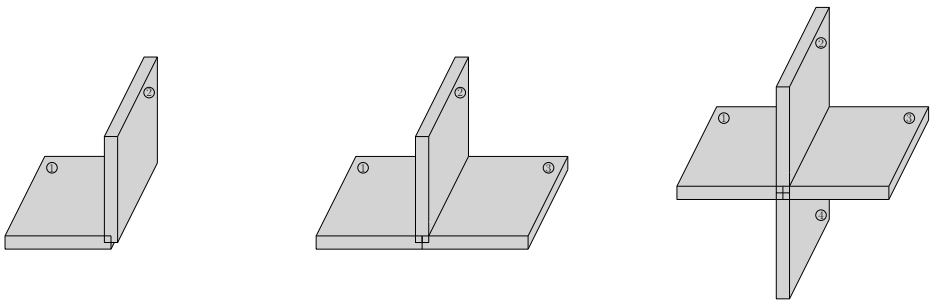

(a) L-junction (b) T-junction (c) X-junction

Figure 3: Different types of junctions

The thickness of plate 1 (and 3) is varied from 0.05 m to 0.4 m. To determine the thickness of the perpendicular plate(s), the ratio of characteristic moment impedances is varied from 0.01 to 300. This sometimes results in an unrealistic thickness for the perpendicular plates(s). Results for thicknesses larger than 0.4 m are ignored. The ratio of characteristic moment impedances $\frac{\psi}{\chi}$ is given by

$$\frac{\psi}{\chi} = \sqrt[4]{\frac{m'_{\perp j} B^3_{\perp j}}{m'_j B^3_j}} \tag{20}$$

where m'_j is the mass per unit area of element j, $m'_{\perp j}$ is the mass per unit area of the element perpendicular to element j, B_j is the bending stiffness of element j and $B_{\perp j}$ is the bending stiffness of the element perpendicular to element j.

Table 1: Material properties

Material	Internal loss factor η_{int} [-]	Density ρ [kg/m^3]	Quasi-longitudinal wavespeed c_{L} [m/s]	Poisson ratio ν [-]
1: Concrete	0.005	2200	3800	0.2
2: Brick	0.01	1750	2700	0.2
3: Aerated concrete	0.0125	800	1900	0.2
4: Lightweight aggregate	0.01	1400	1400	0.2
5: Dense aggregate	0.01	2000	3200	0.2
6: Calcium-silicate	0.01	1800	2500	0.2

Using a set of junctions with the properties described above, the diffuse bending wave transmission coefficient is calculated in one-third octave band centre frequencies from 50 Hz to 3150 Hz with the method described in section 2. Following ISO 12354-1, the low-frequency range is defined as the set of one-third octave bands from 50 Hz to 200 Hz, the mid-frequency range from 250 Hz to 1000 Hz and the high-frequency range from 1250 Hz to 3150 Hz. With the new approach it was found that both methods for determining the direct field dynamic stiffness result in the same transmission coefficient values in the low frequency range. The analytical expressions for the direct field dynamic stiffness are thus used in the low-frequency range since these are more computationally efficient. In the mid- and high-frequency range the direct field dynamic stiffness is determined using 2.5D finite elements combined with perfectly matched layers. A single value for the transmission coefficient is obtained by calculating the arithmetic average in the considered frequency range.

3.1. Low-frequency range

Figure 4 shows the transmission losses found in the low-frequency range with the new approach, together with the regression curves from ISO 12354-1 [10]. Here it can be seen that the new approach results in a prediction for the transmission loss that is generally higher than the regression curve from the international standard, which was determined using a combination of finite elements methods (FEM), spectral finite element methods (SFEM) and wave theory [11]. Wave theory assumes an infinite junction, which results in lower transmission losses compared to the finite element models of finite junction as reported by Hopkins et al. [11]. Figure 4 shows that the junction length has an influence on the transmission loss in the low frequency range. This is due to the bending wavelengths in the plates being large compared to the length of the junction in this frequency range, since in the low frequency range mainly bending waves are transmitted between the plates. Since the influence of the length of the junction can be seen in figure 4, regression curves can be determined where the length of the junction is considered. The independent variable used in the low frequency range is PC, which is the variable used by Hopkins et. al. [11] for determining the regression curves which can also be found in ISO 12354-1 [10]:

$$\mathrm{PC} = \log\left(\frac{\psi}{\chi}\right) \tag{21}$$

where $\frac{\psi}{\chi}$ is the ratio of characteristic moment impedances (see formula 20). Cubic polynomials are used ($A \cdot \mathrm{PC}^3 + B \cdot \mathrm{PC}^2 + C \cdot \mathrm{PC} + D$) to fit regression curves through the data for the transmission losses per junction length. The parameters of the regression curves can be found in table 2, together with the coefficient of determination R^2 of the regression curves. For simplicity of use, single values are used for parameters of the regression curves which only varied slightly for different junction lengths. For the other parameters a logarithmic fit ($E + F \log(L)$) is used to find the parameter of the regression curve for different junction lengths. With these regression curves, coefficients of determination of 0.97 and 0.98 are found for all junction types, indicating a high accuracy of the fit.

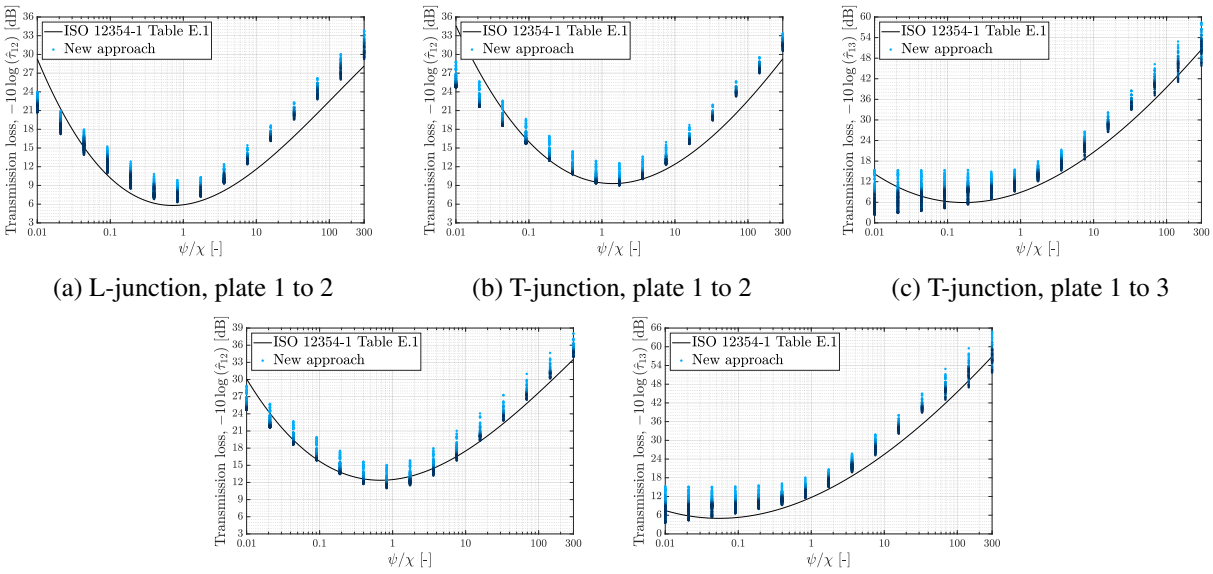

(a) L-junction, plate 1 to 2 (b) T-junction, plate 1 to 2 (c) T-junction, plate 1 to 3

(d) X-junction, plate 1 to 2 (e) X-junction, plate 1 to 3

Figure 4: Results using the new approach in low-frequency range (50-200 Hz) together with the regression curve from ISO 12354-1. Light blue dots correspond to a junction length of 2 m and darkblue to a junction length of 8 m. The colors used for plotting results of intermediate junction lengths are interpolated between light- and darkblue.

Table 2: Parameters of the regression curves and coefficient of determination in the low-frequency range

Junction	Transmission	A	B	C	D	R^2
L	plate 1 to 2	-0.2	3.9	1.3	$10.5 - 2.7\log(L)$	0.97
T	plate 1 to 2	0.2	3.7	-1	$13.4 - 3.7\log(L)$	0.98
T	plate 1 to 3	0.2	$4.0 - 1.7\log(L)$	$6.4 + 2.2\log(L)$	$16.4 - 4.5\log(L)$	0.98
X	plate 1 to 2	-0.1	3.7	1.1	$15.8 - 4.1\log(L)$	0.98
X	plate 1 to 3	-0.2	$4.3 - 1.5\log(L)$	$10 + 0.6\log(L)$	$18.3 - 3.8\log(L)$	0.98

3.2. Mid-frequency range

Results for the transmission losses found in the mid-frequency range can be seen in figure 5. A new variable is introduced for plotting results in this frequency range since previous research has shown that the ratio of characteristic moment impedances is not the best variable for plotting results in the mid- and high-frequency range [12]. The new variable is based on the ratio of characteristic moment impedances but also takes into account the in-plane stiffness of the plates since in the mid-frequency range in-plane waves also influence the vibration transmission across the junction:

$$V_{\mathrm{mid}} = \log\left(\frac{\psi}{\chi}\sqrt{\frac{E_{\perp j}t_{\perp j}}{E_j t_j}}\right) \tag{22}$$

Figure 5 also shown a relation between junction length and transmission loss, thus a similar approach is followed to the low-frequency range. Quadratic regression curves are used ($A \cdot \mathrm{V_{mid}}^2 + B \cdot \mathrm{V_{mid}} + C$) for ease of use since cubic curves barely improved the quality of the fit in this frequency range. The parameters of the regression curves can be found in table 2, together with the coefficient of determination R^2 of the regression curves. Coefficients of determination from 0.95 to 0.98 are found for the different types of junctions.

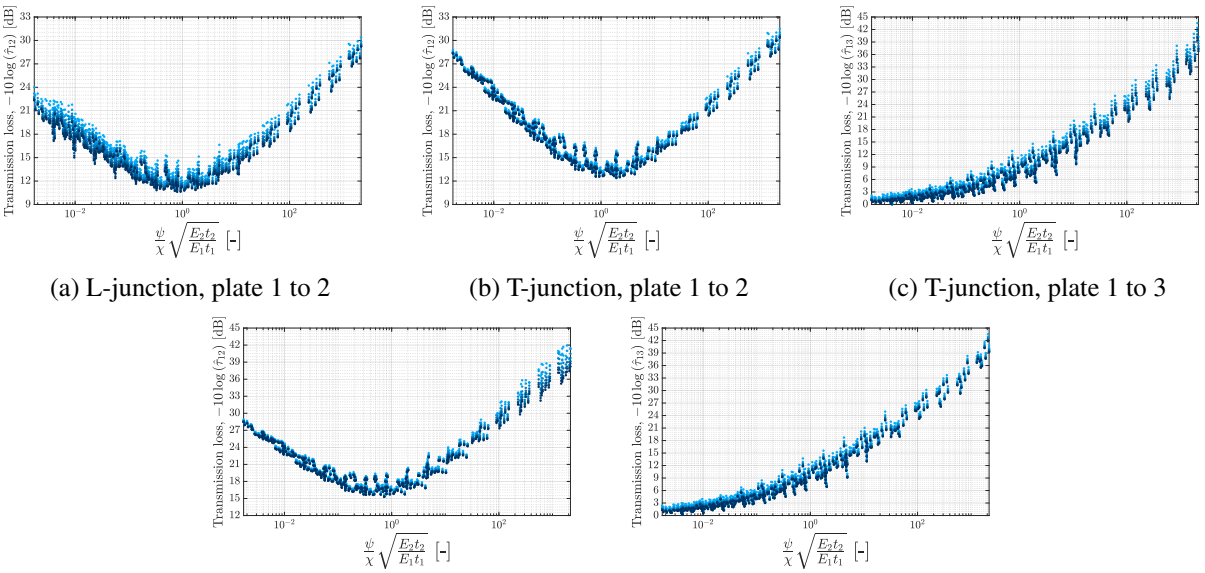

(a) L-junction, plate 1 to 2 (b) T-junction, plate 1 to 2 (c) T-junction, plate 1 to 3

(d) X-junction, plate 1 to 2 (e) X-junction, plate 1 to 3

Figure 5: Results using the new approach in mid-frequency range (250-1000 Hz) together with the regression curve from ISO 12354-1. Light blue dots correspond to a junction length of 2 m and darkblue to a junction length of 8 m. The colors used for plotting results of intermediate junction lengths are interpolated between light- and darkblue.

Table 3: Parameters of the regression curves and coefficient of determination in the mid-frequency range

Junction	Transmission	A	B	C	R^2
L	plate 1 to 2	1.5	$0.2 + 0.2 \log(L)$	$14.4 - 2.6 \log(L)$	0.95
T	plate 1 to 2	1.8	$-0.5 - 0.2 \log(L)$	$15.1 - 1.0 \log(L)$	0.96
T	plate 1 to 3	1.0	$5.8 - 0.8 \log(L)$	$10.1 - 2.9 \log(L)$	0.97
X	plate 1 to 2	1.9	$1.6 - 0.7 \log(L)$	$18.4 - 0.8 \log(L)$	0.95
X	plate 1 to 3	1.0	$5.9 - 0.2 \log(L)$	$11.2 - 2.4 \log(L)$	0.98

3.3. High-frequency range

Finally, results for the high-frequency range can be seen in figure 6. Since in this frequency range in-plane waves have a stronger influence than in the mid-frequency range, again a new variable for plotting results is introduced:

$$V_{\text{high}} = \log\left(\sqrt{\frac{\psi}{\chi}}\left(\frac{E_{\perp j} t_{\perp j}}{E_j t_j}\right)^2\right) \tag{23}$$

Like in the mid-frequency range, quadratic regression curves ($A \cdot \mathrm{V_{high}}^2 + B \cdot \mathrm{V_{high}} + C$) are calculated. The parameters of the regression curves for the different junction types can be found in table 4. In the final column of this table, the coefficient of determination can be found for the different types of junctions. The coefficients of determination in the high-frequency range are slightly lower than in the other frequency ranges, especially for the transmission from plate 1 to plate 2 for a T- and and X-junction. Nevertheless, coefficients of determination of 0.85 and higher are found in the high-frequency range with the new variable.

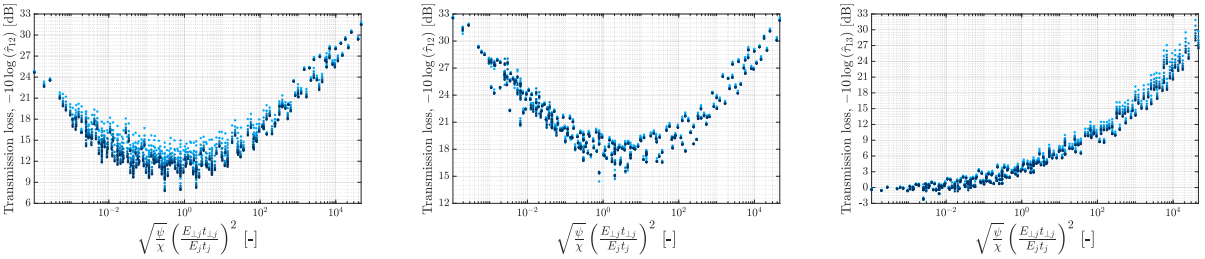

(a) L-junction, plate 1 to 2

(b) T-junction, plate 1 to 2

(c) T-junction, plate 1 to 3

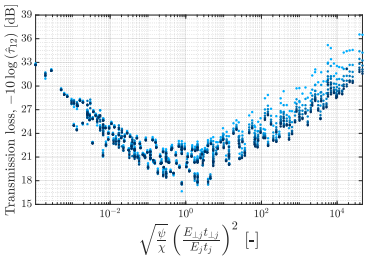

(d) X-junction, plate 1 to 2

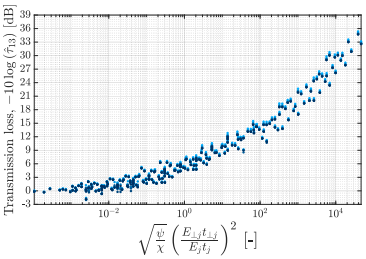

(e) X-junction, plate 1 to 3

Figure 6: Results using the new approach in high-frequency range (1250-3150 Hz) together with the regression curve from ISO 12354-1. Lightblue dots correspond to a junction length of 2 m and darkblue to a junction length of 8 m. The colors used for plotting results of intermediate junction lengths are interpolated between light- and darkblue.

Table 4: Parameters of the regression curves and coefficient of determination in the high-frequency range

Junction	Transmission	A	B	C	R^2
L	plate 1 to 2	0.9	$0.2 + 0.2\log(L)$	$14.8 - 4.5\log(L)$	0.94
T	plate 1 to 2	0.8	-0.9	18.2	0.91
T	plate 1 to 3	0.5	$3.0 - 0.5\log(L)$	$4.1 - 0.9\log(L)$	0.98
X	plate 1 to 2	0.7	$0.3 - 0.7\log(L)$	$21.7 - 1.0\log(L)$	0.85
X	plate 1 to 3	0.6	3.3	5.5	0.98

4. CONCLUSIONS

A new approach for calculating vibration transmission across junctions based on diffuse field reciprocity has been presented, which calculates the transmission coefficient using the coupling loss factor. The coupling loss factor is calculated based on the direct field dynamic stiffness matrices of the plates connected to the junction. The direct field dynamic stiffness matrix of a plate can be determined in multiple ways. Two possible methods were considered in this work, where the first uses thin plate theory to analytically derive the direct field dynamic stiffness matrix of a thin, isotropic, semi-infinite plate in the wavenumber domain. Since the assumption of thin plates is only valid at low frequencies, a second method is considered which uses a combination of 2.5D finite elements and perfectly matched layers to calculate the direct field dynamic stiffness matrix in the wavenumber domain. To transform this result from the wavenumber domain to the spatial domain a correction for the finite junction length is applied.

Due to the computational efficiency of the new approach, vibration transmission across a large set of junctions could be calculated. The results from these simulation could then be used to calculate regression curves and to asses the influence of the length of the junction on the vibration transmission.

In the low-frequency range good fits are found using the ratio of characteristic moment impedances as the independent variable for plotting results. In the mid- and high-frequency ranges, new variables were introduced for plotting the results. The ratio of characteristic moment impedances is based on the bending stiffness and surface mass of the plates connected to the junction. With increasing frequency, in-plane wave become more important for the vibration transmission across the junction. The new variables are thus also based on the in-plane stiffness of the plates connected to the junction.

For all frequency ranges, regression curves are proposed which show a good fit to the data from the simulations. The new regression curves take into account the influence of the length of the junction on the vibration transmission across the junction.

ACKNOWLEDGEMENTS

The research presented in this paper has been performed within the frame of the VirBAcous project (project ID 714591) "Virtual building acoustics: a robust and efficient analysis and optimization framework for noise transmission reduction" funded by the European Research Council in the form of an ERC Starting Grant. The financial support is gratefully acknowledged.

REFERENCES

[1] C. Hopkins. *Sound insulation*. Elsevier Ltd., Oxford, 2007.

[2] R.J.M. Craik. *Sound transmission through buildings using statistical energy analysis*. Gower, Aldershot, UK, 1996.

[3] L. Cremer and M. Heckl. *Structure-borne sound: Structural vibrations and sound radiation at audio frequencies*. Springer, Berlin, 2nd edition, 1988.

[4] R. S. Langley and K. H. Heron. Elastic wave transmission through plate/beam junctions. *Journal of Sound and Vibration*, 143(2):241–253, 1990.

[5] P.J. Shorter and R.S. Langley. Vibro-acoustic analysis of complex systems. *Journal of Sound and Vibration*, 288(3):669–699, 2005.

[6] R. S. Langley. A derivation of the coupling loss factors used in statistical energy analysis. *Journal of Sound and Vibration*, 141(2):207–219, 1990.

[7] S. François, M. Schevenels, G. Lombaert, P. Galvín, and G. Degrande. A 2.5D coupled FE-BE methodology for the dynamic interaction between longitudinally invariant structures and a layered halfspace. 199(23-24):1536–1548, 2010.

[8] U. Basu and A.K. Chopra. Perfectly matched layers for time-harmonic elastodynamics of unbounded domains: theory and finite-element implementation. *Computer Methods in Applied Mechanics and Engineering*, 192(11-12):1337–1375, 2003.

[9] V. Cotoni, P. Shorter, and R. Langley. Numerical and experimental validation of a hybrid finite element-statistical energy analysis method. *Journal of the Acoustical Society of America*, 122(1):259–270, 2007.

[10] International Organization for Standardization. *ISO 12354-1:2017: Building Acoustics - Estimation of acoustic performance of buildings from the performance of elements - Part 1: Airborne sound insulation between rooms*, 2017.

[11] C. Hopkins, C. Crispin, J. Poblet-Puig, and C. Guigou-Carter. Regression curves for vibration transmission across junctions of heavyweight walls and floors based on finite element methods and wave theory. *Applied Acoustics*, 113:7–21, 2016.

[12] W. Stalmans, C. Van hoorickx, and E.P.B. Reynders. Predicting the diffuse vibration transmission across finite junctions between thick plates. In *Proceedings of the 50th International Congress and Exposition on Noise Control Engineering, Inter-Noise 2021*, Washington D.C., August 2021. Paper submitted.